

# RSC Advances



This is an *Accepted Manuscript*, which has been through the Royal Society of Chemistry peer review process and has been accepted for publication.

*Accepted Manuscripts* are published online shortly after acceptance, before technical editing, formatting and proof reading. Using this free service, authors can make their results available to the community, in citable form, before we publish the edited article. This *Accepted Manuscript* will be replaced by the edited, formatted and paginated article as soon as this is available.

You can find more information about *Accepted Manuscripts* in the [Information for Authors](#).

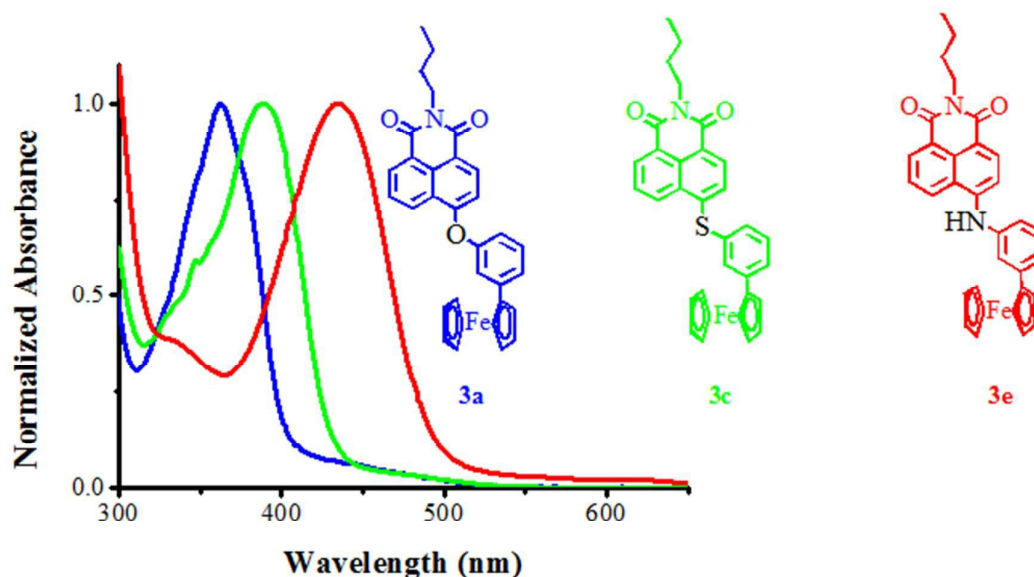
Please note that technical editing may introduce minor changes to the text and/or graphics, which may alter content. The journal's standard [Terms & Conditions](#) and the [Ethical guidelines](#) still apply. In no event shall the Royal Society of Chemistry be held responsible for any errors or omissions in this *Accepted Manuscript* or any consequences arising from the use of any information it contains.

## Heteroatom–Connected Ferrocenyl Substituted Naphthalimides

T. Sheshashena Reddy, Ramesh Maragani, Bhausaheb Dhokale, Shaikh M. Mobin,  
Rajneesh Misra\*

Department of Chemistry, Indian Institute of Technology Indore, Indore 452017, India.

Table of Content graphic



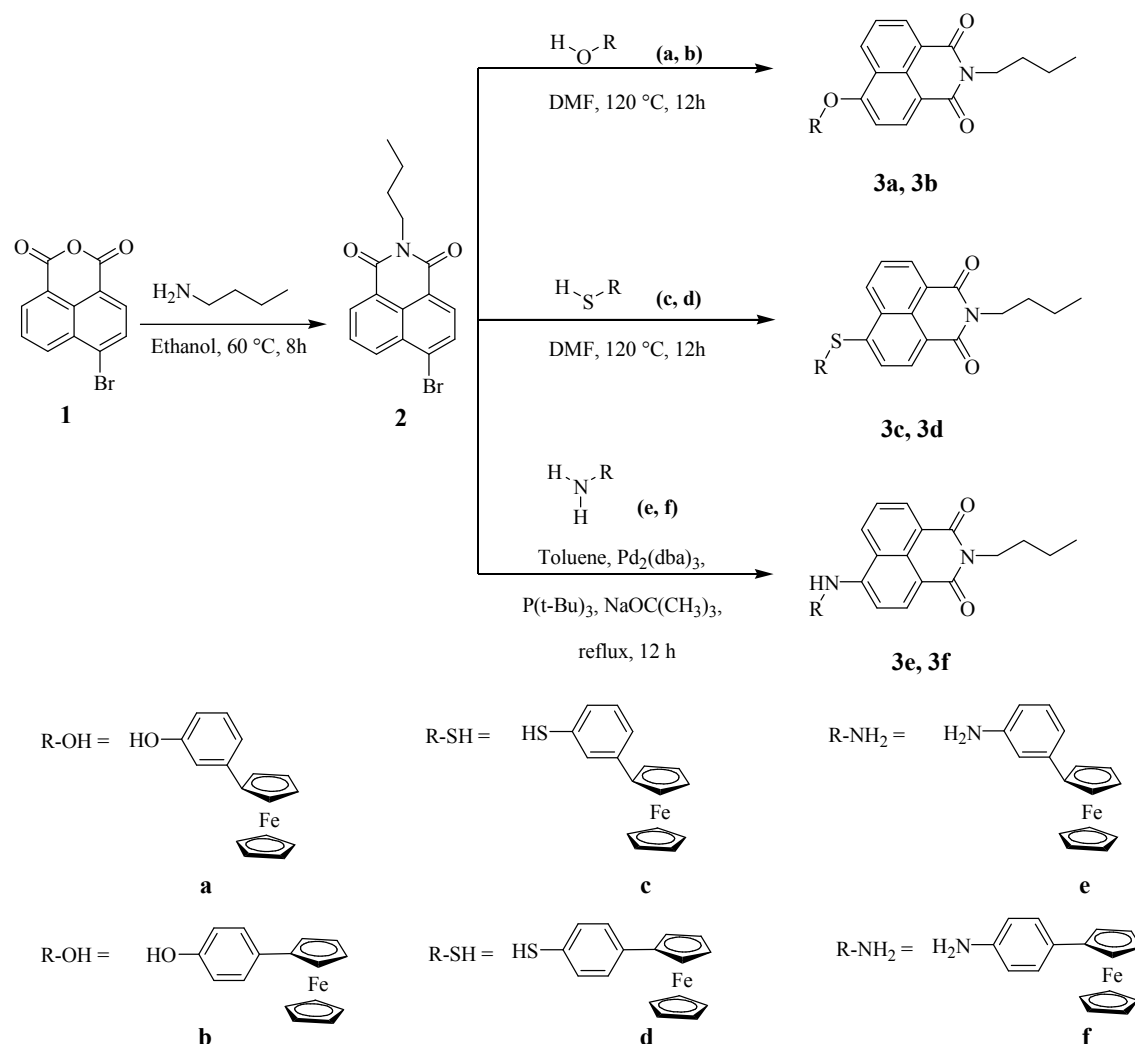
**Abstract:** A family of heteroatom (oxygen, sulphur and nitrogen) connected ferrocenyl naphthalimides **3a–3f** were designed and synthesized by the nucleophilic aromatic substitution and Buchwald coupling reactions. The effects of heteroatom and ferrocenyl group on the photonic and electrochemical properties of the ferrocenyl naphthalimides were explored. The electronic absorption spectra of the ferrocenyl naphthalimides **3a–3f** show red shifted absorption as compared to 4-bromonaphthalimide **2**. The nitrogen atom connected FcNMI (**3e** and **3f**) show considerable red shift, whereas oxygen and sulphur connected FcNMIs (**3a–3d**) show moderate red shift. The computational calculations show good agreement with the experimental results. The ferrocenyl naphthalimide containing nitrogen atom (**3e** and **3f**) show high thermal stability compared to oxygen and sulphur containing dyes **3a–3d**. The single crystal X-ray structure of **3a** and **3c** are reported and these crystal structures forms 2-D network.

**Introduction:**

In last decade substantial effort has been made in the design and synthesis of functional materials exhibiting high optoelectronic performance.<sup>1</sup> Naphthalimide dyes are widely studied functional materials.<sup>2</sup> 1,8-Naphthalimide derivatives exhibits strong fluorescence and large Stokes shift, high thermal and chemical stability.<sup>2a</sup> These properties make them attractive candidate for wide range of applications in laser dyes, organic light emitting diodes, liquid crystals, sensors, organic photovoltaics, and in biomedicines.<sup>2b,3-8</sup> The photonic properties of the 1,8-naphthalimide derivatives can be tuned by the functionalization at C-4 position.<sup>9</sup> Large number of groups have explored C-4 functionalized 1,8-naphthalimide for fundamental spectroscopic studies, biomedical studies and optoelectronics.<sup>8,10,11</sup> Ferrocene is a strong donor and widely studied in material applications.<sup>12</sup> Robinson *et al.*, have reported a set of *N*-(ferrocenyl)-naphthalimides and *N,N'*-diferoenyl-naphthalimides by the condensation reaction of naphthalic anhydrides with ferrocenyl amines.<sup>13</sup> The ferrocenyl unit show poor electronic communication with the naphthalimide unit due to node at N-imide atom. The same group has reported a series of 4-substituted naphthalimide (ethenylferrocene, ethynylferrocene, piperidinyl) derivatives with *N*-ferrocenyl head groups.<sup>14</sup> Simpson *et al.*, synthesized 4-(ethenylferrocene) substituted naphthalimides with spacers (4,4'-biphenyl, 1,4-phenyl, 9,10-anthracenyl).<sup>15</sup> The spacer in these dyads showed minimum effect on the photophysical and electrochemical properties. The TD-DFT studies of these dyads revealed the existence of low-energy near-infrared bands.<sup>16</sup> Recently, Chinapang *et al.*, reported ferrocenyl functionalized 1,8-naphthalimide as turn-on fluorescent sensor for gold ion.<sup>17</sup> Our group is involved in the design and synthesis of ferrocenyl based Donor-Acceptor systems for electronic and photonic applications.<sup>18</sup> Recently we have reported effect of heteroatom and ferrocene group on the heteroatom connected ferrocenyl BODIPYs.<sup>19</sup> We have explored the effect of ferrocenyl donor on variety of acceptors. In continuation of our research on ferrocenyl system, we were further interested to see the effect of heteroatom (O, N and S) and the ferrocenyl unit of the photonic and electrochemical properties of the 1,8-naphthalimide. Therefore *meta* and *para* linked ferrocenyl phenols (**a** and **b**), ferrocenyl thiophenols (**c** and **d**) and ferrocenyl anilines (**e** and **f**) were designed and treated with 4-bromo-1,8-naphthalimide.

**Results and discussion:** The ferrocenyl naphthalimides (FcNMIs) **3a-3f** were synthesized by the nucleophilic aromatic substitution and Buchwald coupling reactions (Scheme 1). The 4-bromo-1,8-naphthalic anhydride **1** was reacted with *n*-butyl amine in ethanol solvent at 60 °C for 8 h, which resulted 4-bromonaphthalimide **2** in 88% yield. The ferrocenyl phenols (**a**

and **b**) were synthesized by the diazotization reaction of the aminophenols with ferrocene. The ferrocenyl thiophenols (**c** and **d**) were synthesized by the diazotization reaction of aminothiophenols with ferrocene in 20% sulfuric acid and toluene solvent mixture stirred for 24 h at room temperature (Supporting information, Scheme S1). The ferrocenyl anilines (**e** and **f**) were synthesized by the diazotization reaction of nitroanilines with ferrocene followed by reduction with Sn/HCl.<sup>19</sup> The oxygen and sulphur atom-connected FcNMI **3a–3d** were synthesized by the aromatic nucleophilic substitution reaction of **2** with the corresponding ferrocenyl phenols (**a** and **b**) and ferrocenyl thiophenols (**c** and **d**) in N,N'-dimethylformamide (DMF) solvent and K<sub>2</sub>CO<sub>3</sub> as base at 120 °C for 12 h, which resulted **3a**, **3b**, **3c** and **3d** in 74%, 77%, 67% and 70% yields, respectively. The nitrogen atom-connected FcNMI **3e** and **3f** were synthesized by the Buchwald coupling reaction. The Pd-catalyzed Buchwald coupling reaction of **2** with ferrocenyl anilines (**e** and **f**) resulted **3e** and **3f** in 63% and 68% yields, respectively.



**Scheme 1:** Synthesis of heteroatom-connected ferrocenyl naphthalimides **3a–3f**.

The FcNMIs **3a–3f** were well characterized by  $^1\text{H}$ ,  $^{13}\text{C}$  NMR and HRMS techniques (Supporting Information, Figures S1–S25). The FcNMIs **3a** and **3c** were also characterized by the single crystal X-ray technique. The  $^1\text{H}$  NMR spectra of the **3a–3f** show, ferrocenyl protons in the 4.68–4.07 ppm region, five aromatic protons of naphthalene ring as four doublets and one triplet 8.71–7.33 ppm and phenyl protons were observed in the region 8.01–6.95 ppm.

**Thermogravimetric analysis:** Thermal stability is one of the important parameter for the optoelectronic applications of materials. The thermal properties of the FcNMIs **3a–3f** were investigated by thermogravimetric analysis (TGA) with a heating rate of  $10\text{ }^\circ\text{C min}^{-1}$  under an inert atmosphere (Figure 1). The thermal decomposition temperatures ( $T_d$ ) at 5% weight loss are shown in Table 1. The trend of thermal stability follows the order **3a** > **3c** ≈ **3f** > **3b** > **3e** > **3d**. The sulphur atom containing FcNMIs **3d** and **3c** show a sudden weight loss of 70%

and 80% at 475 °C and 456 °C respectively. The oxygen atom containing FcNMIs **3b** and **3a** show a sudden weight loss of 75% at 468 °C and 463 °C respectively. The nitrogen atom containing FcNMIs **3f** and **3e** show a sudden weight loss of 38% and 25% at 435 °C and 387 °C respectively. These results suggest that the *para* isomers are thermally stable than the *meta* isomers.

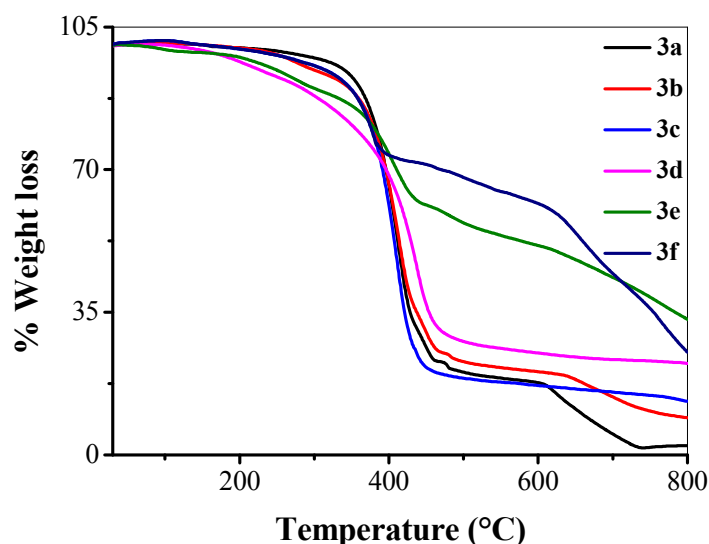


**Figure 1:** TGA plots of the FcNMIs **3a–3f**.

**UV-visible studies:** The UV–vis absorption spectra of the FcNMIs **3a–3f** were recorded in dichloromethane at room temperature (Figure 2) and the corresponding data are given in Table 1. The 4-bromonaphthalimide **2** absorbs at 342 nm with a shoulder at 356 nm which can be attributed to the  $\pi$ – $\pi^*$  electronic transition. The FcNMIs **3a–3f** show red shifted absorption bands at 363 nm (**3a**), 363 nm (**3b**), 386 nm (**3c**), 389 nm (**3d**), 435 nm (**3e**) and 445 nm (**3f**) respectively. The oxygen connected FcNMIs **3a** and **3b** exhibits 7 nm red shift, whereas the sulphur connected FcNMIs **3c** and **3d** show 33 nm and 30 nm red shift, and nitrogen connected FcNMIs **3e** and **3f** show 79 nm and 89 nm red shift compared to 4-bromonaphthalimide **2**. The red shift in the absorption maximum of FcNMIs **3a–3f** can be understood in term of delocalization of lone pair electron of hetero atom into the naphthalimide ring (Supporting Information, Figure S26). The nitrogen connected FcNMIs **3e** and **3f** show red shift in the absorption spectra as compared to the oxygen and sulphur connected FcNMIs, which may be due to the delocalization of lone pair electron of nitrogen into the naphthalimide ring.<sup>10</sup> The extent of delocalization of the lone pair of electrons in the

FCNMI 3a–3f can be explained by the molecular electrostatic potential maps (Supporting Information, Figure S26). In the FCNMI 3e and 3f molecular electrostatic potential map the nitrogen atom carries positive potential (blue colour), whereas, FCNMI 3a–3d, the oxygen and sulphur atom does not carry any positive potential. The heteroatom connected FCNMI 3a–3f were found to be non-emissive. The quenching of fluorescence can be attributed to the fast nonradiative deactivation of the excited state with intramolecular charge transfer from the donor ferrocenyl unit to the acceptor naphthalimide moiety.<sup>18,19</sup>

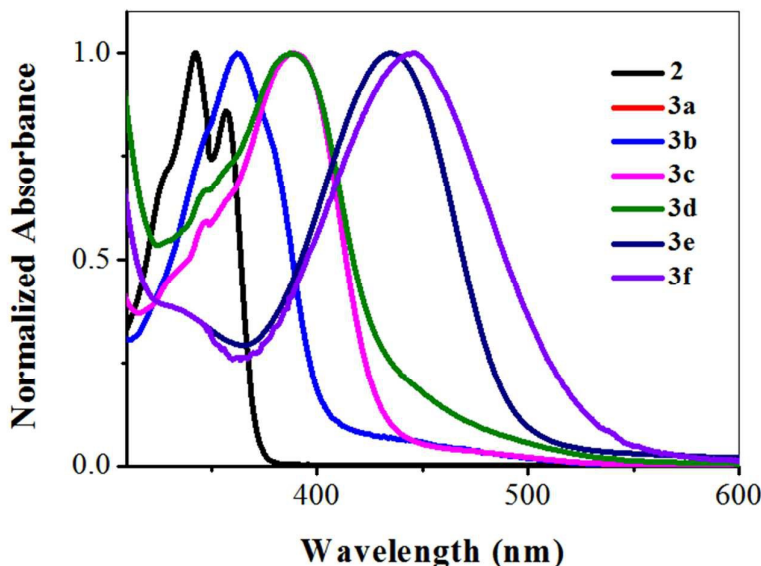


**Figure 2:** Normalized electronic absorption spectra of **2** and **3a–3f**.

**Electrochemical Properties:** The electrochemical properties of the heteroatom-connected FCNMI 3a–3f were explored by cyclic voltammetric (CV) and the results are shown in Table 1 (Supporting Information, Figure S27). The representative cyclic voltammograms of FCNMI 3a and 3b are shown in Figure 3. The heteroatom-connected ferrocenyl substituted naphthalimides show one reversible oxidation wave in the region 0.03–0.07 V corresponding to the oxidation of ferrocene to ferrocenium ion (Fc/Fc<sup>+</sup>). The FCNMI 3a–3f exhibit one irreversible reduction wave in the region –1.30 V to –1.37 V, attributed to the acceptor naphthalimide unit. The trend in the oxidation potential of the ferrocenyl moiety in the FCNMI 3a–3f follows the order 3f > 3e > 3a > 3b > 3c > 3d, whereas the reduction potential of the FCNMI 3a–3f follows the order 3b > 3a > 3d > 3c > 3f > 3e. The nitrogen connected FCNMI shows harder oxidation potential as compared to the oxygen and sulphur connected FCNMI, which may be due to the delocalization of lone pair electron of nitrogen into the naphthalimide ring. The extent of delocalization of the lone pair of electrons in the FCNMI 3a–3f can be explained by the molecular electrostatic potential maps (Supporting

Information, Figure S26). In the FCNMs **3e** and **3f** molecular electrostatic potential map the nitrogen atom carries positive potential (blue colour), whereas, FCNMs **3a–3d**, the oxygen and sulphur atom does not carries any positive potential. These observations are in good agreement with the optical and electrochemical properties. The oxygen and sulphur *meta* position connected FcNMs shows harder oxidation potential as compared to the *para* connected FcNMs oxidation potentials. In the case of nitrogen connected FcNMs the *para* connected FcNMs shows harder oxidation potential as compared to the *meta* connected FcNMs oxidation potential.

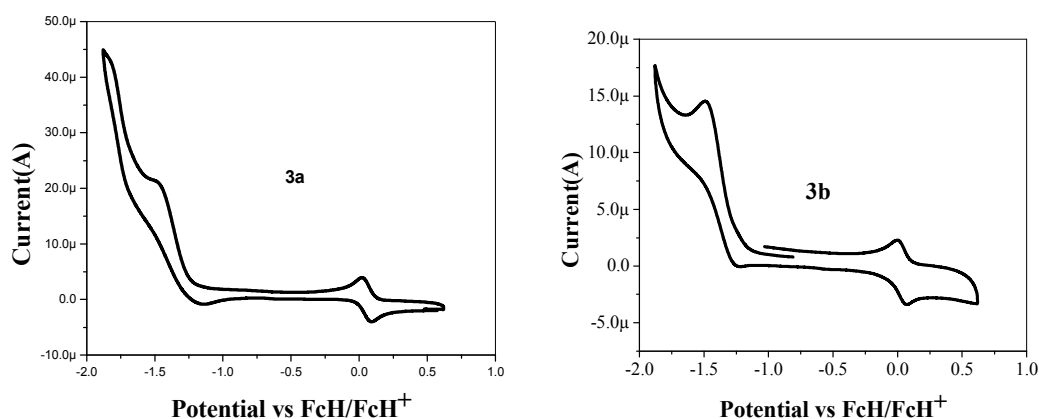


**Figure 3:** Cyclic voltammograms of the **3a** and **3b** at  $1.0 \times 10^{-4}$  M concentration in dichloromethane recorded at a scan rate of  $100 \text{ mVs}^{-1}$ .

**Table 1:** Photophysical and electrochemical properties of **3a–3f**.

FcNMs	Experimental <sup>a</sup> $\lambda_{\text{max}}(\text{nm})^b$ ( $\epsilon$ ) <sup>c</sup>	Theoretical $\lambda_{\text{max}}(\text{nm})$	$E_{\text{oxid}}(\text{V})^d$	$E_{\text{red}}(\text{V})^d$	$T_d^e$ (°C)
<b>3a</b>	363 (21746)	360	0.057	1.36	338
<b>3b</b>	363 (21587)	363	0.033	1.37	296
<b>3c</b>	386 (19816)	389	0.045	1.35	313
<b>3d</b>	389 (19258)	386	0.030	1.36	221
<b>3e</b>	435 (17591)	439	0.065	1.30	243
<b>3f</b>	445 (18225)	469	0.071	1.31	313

<sup>a</sup>Measured in  $\text{CH}_2\text{Cl}_2$ . <sup>b</sup>Absorption maxima. <sup>c</sup>Extinction coefficient recorded at  $\lambda_{\text{abs(max)}}$ .

<sup>d</sup>Electrochemical analysis was performed at room temperature  $25^\circ\text{C}$  and in a 0.1 M solution

of Bu<sub>4</sub>NPF<sub>6</sub> in CH<sub>2</sub>Cl<sub>2</sub> at 100 mVs<sup>-1</sup> scan rate versus Fc/Fc<sup>+</sup>. Tem All potentials are expressed in volts (V).<sup>o</sup>Thermal decomposition temperature at 5% weight loss, determined by TGA.

**Theoretical Calculations:** In order to understand the photophysical and electrochemical properties of the FcNMI 3a–3f, the time dependent density functional (TD–DFT) calculations<sup>20</sup> were performed by using Gaussian 09 program 6–31G\*\* for C, N, H and LANL2DZ for Fe<sup>21</sup> at B3LYP level.<sup>22</sup>

The FcNMI 3a–3f experimental and computed (TD–DFT: B3LYP) (UV–vis) absorption data are represented in Figure 4 (Supporting Information, Figure S28). The strong absorption band of 3a and 3b calculated at B3LYP levels are 363 nm, 360 nm respectively. The experimental values for this transition are 363 nm for 3a, as well as 3b both. The experimental values are in good agreement with the TD–DFT/B3LYP values. The individual TDDFT–predicted graphs with excitation energies and oscillator strengths of FCNMIs were given in supporting information (Figure S29–S34).

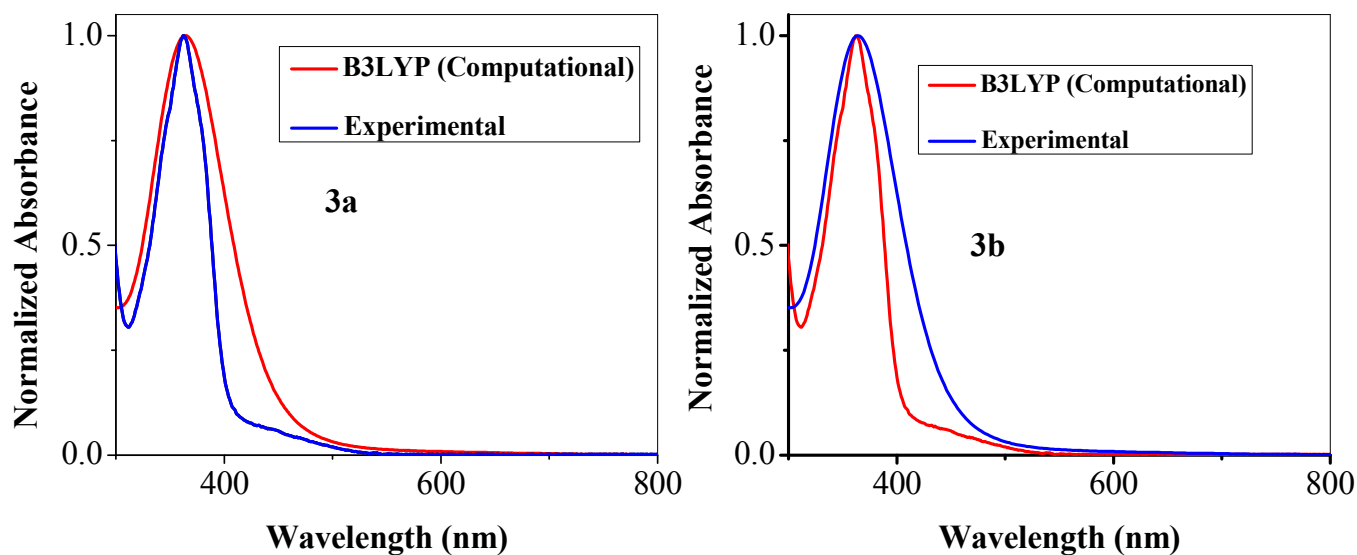


**Figure 4:** The comparison of experimental and calculated (TD–DFT at B3LYP and) absorption spectra of 3a and 3b in DCM solution.

The frontier molecular orbitals of the FcNMI 3a–3f are displayed in Figure 5 (Supporting Information, Figure S35). In the FcNMI 3a–3f the HOMO is localized on the ferrocenyl and phenyl groups and HOMO–1 is localized only on the ferrocenyl group, whereas the LUMO is

located on the naphthalimide group. The HOMO-1→LUMO transition reflects the strong donor-acceptor interactions. The major absorption band in the electronic absorption spectra of the FcNMI 3a-3d and 3f corresponds to HOMO-1→LUMO, whereas FcNMI 3e shows major transition from HOMO-2→LUMO (Table 2).

**Table 2:** Computed vertical transition energies, their Oscillator strengths (*f*), configurations and transitions for the FcNMIs 3a-3f.

FcNMIs	Theory	$\lambda_{\max}$ (nm)	<i>f</i>	Configuration	Transition
3a	B3LYP (DCM)	360	0.3509	HOMO-2→LUMO (100%)	$\pi-\pi^*$
3b	B3LYP (DCM)	363	0.2886	HOMO-2→LUMO (100%)	$\pi-\pi^*$
3c	B3LYP (DCM)	386	0.3586	HOMO-2→LUMO (100%)	$\pi-\pi^*$
3d	B3LYP (DCM)	389	0.4315	HOMO-2→LUMO (100%)	$\pi-\pi^*$
3e	B3LYP (DCM)	439	0.3045	HOMO-2→LUMO (100%)	$\pi-\pi^*$
3f	B3LYP (DCM)	469	0.3507	HOMO-2→LUMO (100%)	$\pi-\pi^*$

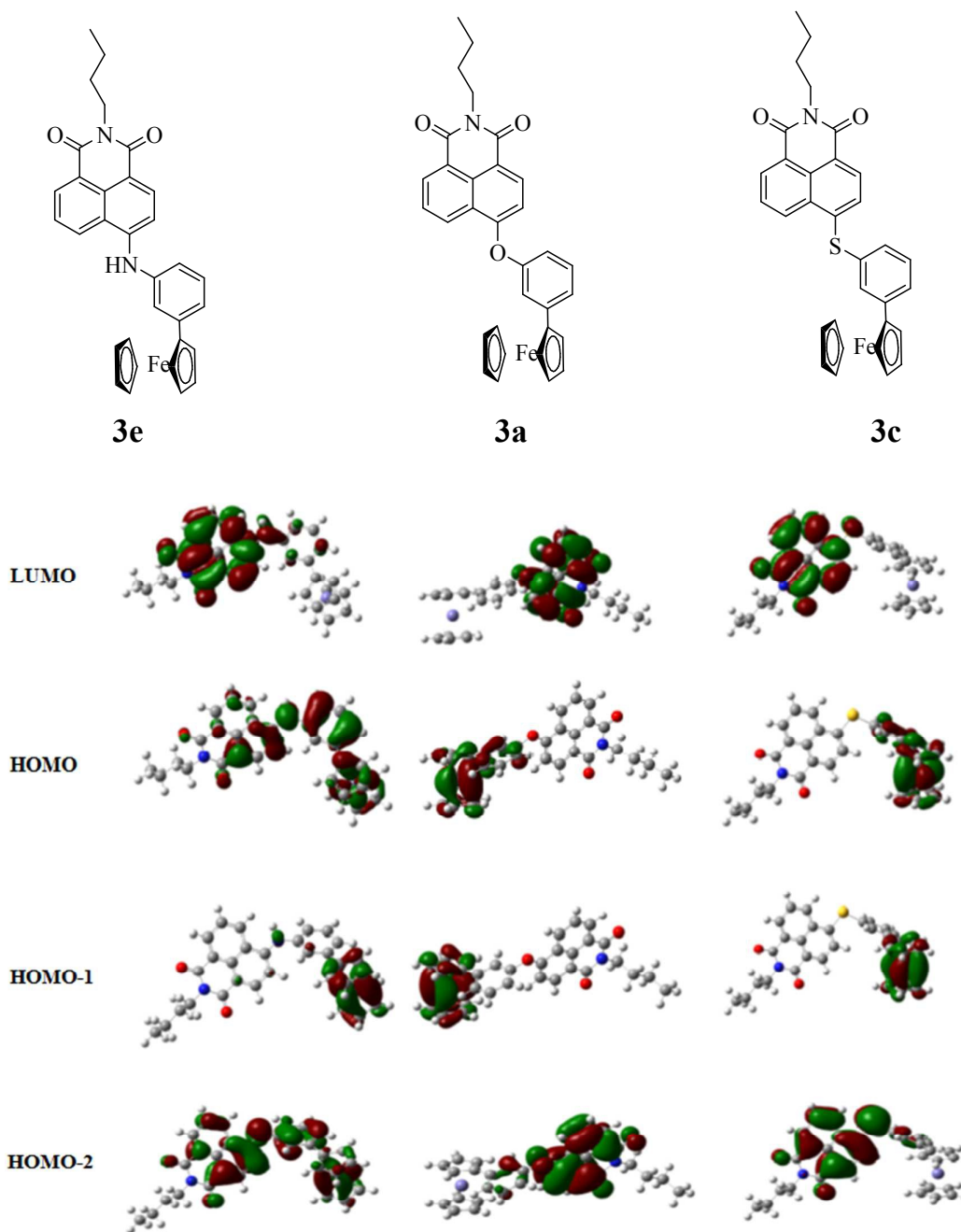


**Figure 5:** The energy level diagram of the frontier molecular orbitals (HOMO-2 to LUMO) of the FcNMIs **3e**, **3a** and **3c** calculated using B3LYP level of TD-DFT theory.

The energy level diagram of the frontier molecular orbitals of the FcNMIs **2**, **3a-3f** was estimated by DFT-B3LYP calculations and are shown in Figure 6. In the FcNMIs **3a-3f**, the sulphur connected FcNMIs **3c** and **3d** the HOMO and LUMO are lower in energy in comparison to the oxygen and nitrogen connected FcNMIs **3a**, **3b**, **3e** and **3f**. The sulphur

atom at the naphthalimide 4-position of the FcNMIs stabilizes the HOMO and LUMO in comparison to an O and N atoms.

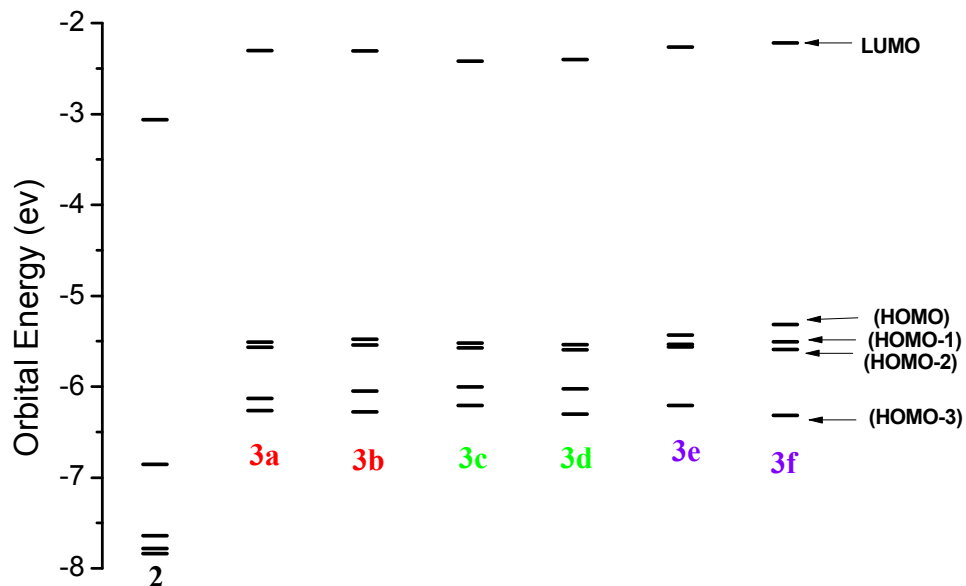


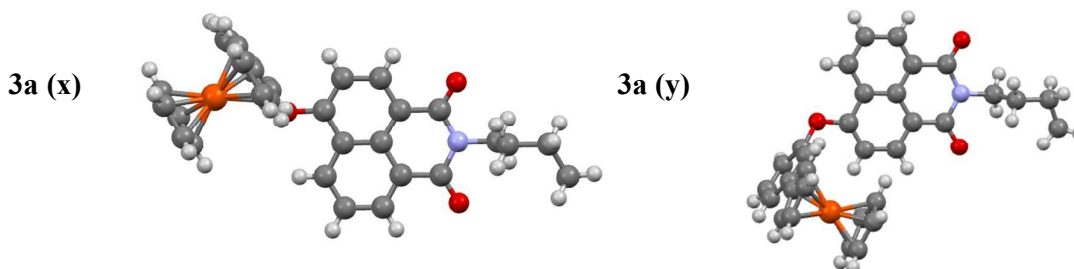
**Figure 6:** The energy level diagram of the frontier molecular orbitals (HOMO–3 to LUMO) of the FcNMIs **3a–3f** calculated using B3LYP level of TD–DFT theory.

The HOMO–LUMO gap for FcNMIs **3a–3f** calculated at B3LYP level are 3.21, 3.16, 3.10, 3.13, 3.16, 3.10 eV respectively (Table 3). The optical band gap values for FcNMIs **3a–3f** are 3.05, 3.05, 2.85, 2.63, 2.45, 2.29 eV respectively. Therefore, the optical HOMO–LUMO gap values are good agreement with values calculated by B3LYP method and follows the order **3a > 3b > 3e > 3d > 3c > 3f**.

**Table 3:** The comparison of the HOMO–LUMO gap of the FcNMIs **3a–3f** using B3LYP level of theory.

FcNMIs	B3LYP (eV)			Optical HOMO–LUMO gap (eV)
	HOMO	LUMO	E <sub>Gap</sub>	
<b>3a</b>	5.51	2.30	3.21	3.05
<b>3b</b>	5.47	2.30	3.17	3.05
<b>3c</b>	5.52	2.41	3.11	2.85
<b>3d</b>	5.53	2.40	3.13	2.63
<b>3e</b>	5.43	2.26	3.17	2.45
<b>3f</b>	5.31	2.21	3.10	2.29

**Single–Crystal X–ray Analysis:** The crystal structures of FcNMIs **3a** and **3c** were obtained by slow diffusion of ethanol into dichloromethane solution at room temperature. The FcNMI **3a** and **3c** crystallizes in the triclinic *P*–1 space group. In FcNMI **3a** and **3c** there are two independent molecules (x and y) in an asymmetric unit, with slight variations in their bond lengths (Figure 7). In FcNMI **3a** and **3c** cyclopentadienyl rings of the ferrocenyl moieties show skew–eclipsed conformation (Supporting Information, Figure S36). The crystal structure data refinement parameters and selected bond lengths are given in Table S1 (Supporting Information) and Table S2–S3 (Supporting Information) respectively.



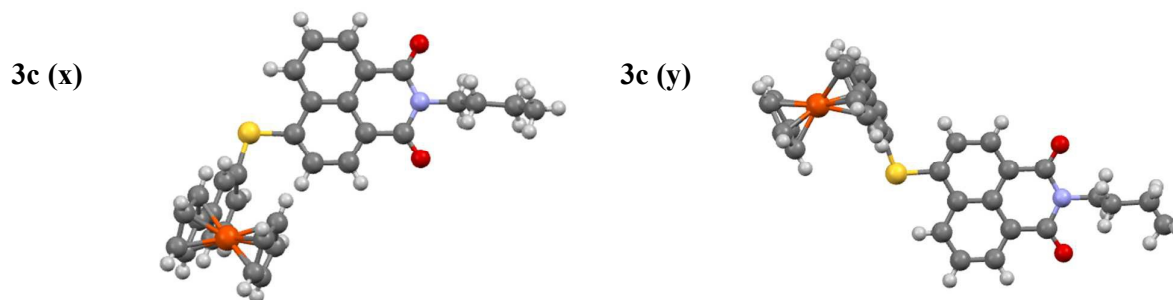


**Figure 7:** Crystal structures of the FcNMIs **3a** and **3c**: x and y represents two different molecules in an asymmetric unit.

In the crystal structure of the FcNMI **3a** there are two molecules (x and y) in an asymmetric unit which differ in the torsion angles of the cyclopentadienyl rings. x and y molecules torsion angle are  $6.42^\circ$  and  $4.93^\circ$  respectively. FcNMI **3a** shows various C–H $\cdots\pi$  interactions. Ferrocenyl carbons C55, C56 and C58 forms C–H $\cdots\pi$  interaction with H27, H32 and H4 hydrogen atoms with 3.264 Å, 2.852 Å and 2.709 Å bond lengths respectively. Ferrocenyl carbon C30 forms C–H $\cdots\pi$  interaction with H53b hydrogen atom with 2.895 Å bond length. Ferrocenyl carbon C64 forms C–H $\cdots\pi$  interaction with naphthalene ring H14 and H5 hydrogen atoms with 2.851 Å and 2.788 Å bond lengths respectively. Naphthalene ring C9 carbon atom forms  $\pi\cdots\pi$  interactions with carbonyl carbon C9 atom with 3.319 Å bond length. Naphthalene ring C8 carbon atom forms C–H $\cdots\pi$  interaction with butyl chain H51B hydrogen atom with 2.830 Å bond length. These supramolecular C–H $\cdots\pi$  and  $\pi\cdots\pi$  interactions in FcNMI **3a**, leads to the formation of 2–D network (Figure S37).

In the crystal structure of the FcNMI **3c** there are two molecules (x and y) in an asymmetric unit which differ in the torsion angles of the cyclopentadienyl rings. x and y molecules torsion angles are  $4.94^\circ$  and  $0.52^\circ$  respectively. FcNMI **3c** shows various C–H $\cdots\pi$  interactions and one  $\pi\cdots\pi$  interaction. Ferrocenyl carbons C24 and C27 forms C–H $\cdots\pi$  interaction with H56 and H61 hydrogen atoms with 2.662 Å and 2.777 Å bond lengths respectively. Ferrocenyl carbon C29 forms C–H $\cdots\pi$  interaction with H41 hydrogen atom with 2.753 Å bond length. Ferrocenyl carbon C32 atom forms  $\pi\cdots\pi$  interactions with same carbon atom with 3.385 Å bond length. These supramolecular C–H $\cdots\pi$  and  $\pi\cdots\pi$  interactions in FcNMI **3c**, leads to the formation of 2–D network (Figure S38).

## Conclusions

In summary, we have described the synthesis of heteroatom-connected ferrocenyl naphthalimides (**3a–3f**) by the nucleophilic aromatic substitution and Buchwald coupling reactions. The nature of the heteroatom perturbs the optical, electrochemical, and thermal properties of the FcNMI substantially. The electronic absorption spectra of the nitrogen heteroatom FcNMIs **3e** and **3f** show considerable red shift compared to the oxygen and sulphur due to the delocalization of the lone pair electrons of the heteroatom to the naphthalimide unit. The TD-DFT calculations show strong donor-acceptor interactions and are in good agreement with the experimental results. The crystal structures of the FcNMIs **3a** and **3c** show C–H $\cdots\pi$  and  $\pi\cdots\pi$  supramolecular interactions and forms 2–D network.

## Acknowledgements:

The work was supported by DST, and CSIR Govt. of India, New Delhi. TSSR thank the IIT Indore for fellowship. We are grateful to the Sophisticated Instrumentation Centre (SIC), IIT Indore.

## Corresponding Author

\*E-mail: [rajneeshmisra@iiti.ac.in](mailto:rajneeshmisra@iiti.ac.in).

Tel.: +91 7312438710; fax: +91 7312361482.

## Supporting Information

The  $^1\text{H}$  NMR,  $^{13}\text{C}$  NMR, HRMS spectra, cyclic voltammograms, UV-vis graphs, and DFT calculations, crystallographic data for **3a** and **3c**, tables, scheme, general experimental section, and CIF files for **3a** and **3c** are provided.

## Experimental data:

**Synthesis of 6-bromo-2-butyl-benzo[de]isoquinoline-1,3-dione 2:** 6-Bromobenzo[de]-isochromene-1,3-dione (1 g, 3.62 mmol) was dissolved in 15 mL ethanol. Then n-butyl amine (0.29 g, 3.98 mmol) was added, and the mixture was stirred at 60°C for 8 h. The mixture was cooled to room temperature and evaporated in vacuum to obtain the residue. Then the residue was purified on silica gel column chromatography employing hexane: ethyl acetate (19:1, V/V) to provide **2**. Yield: 1.06 g, 88%.  $^1\text{H}$  NMR (400 MHz,  $\text{CDCl}_3$ ):  $\delta$  = 8.65 (d,  $J=6.52$ , 1H, aromatic), 8.55 (d,  $J=8.28$ , 1H, aromatic), 8.40 (d,  $J=7.78$ , 1H, aromatic), 8.03 (d,  $J=7.78$ , 1H, aromatic), 7.84 (t,  $J=7.52$ , 1H, aromatic), 4.16 (t,  $J=7.52$ , 2H,  $-\text{NCH}_2$ ), 1.74–1.67 (m, 2H,  $-\text{CH}_2$ ), 1.49–1.39 (m, 2H,  $-\text{CH}_2$ ), 0.97 (t,  $J=7.27$ , 3H,  $-\text{CH}_3$ ).  $^{13}\text{C}$  (100 MHz,  $\text{CDCl}_3$ ):  $\delta$  163.6, 163.6, 133.2, 132.0, 131.1, 131.0, 130.5, 130.1, 128.9, 128.0, 123.1, 122.2, 40.3, 30.1, 20.3, 13.8. Mass spectral data:  $m/z$  ( $\text{M}+\text{Na}$ ) = 354.01 ( $\text{M}+1$ ).

**General procedure for the synthesis of c, d:** In a 500 mL round bottom flask 3/4-aminothiophenol (3 g, 23.96 mmol) was dissolved in 30 mL of 20% sulfuric acid. The solution was cooled to 0°C in an ice bath. Sodium nitrite (1.65 g, 23.96 mmol) in 15 mL water was added over 15 minutes. The mixture was stirred for 30 minutes as the diazonium salt formed. Ferrocene (4.45 g, 23.96 mmol) was dissolved in 100 mL solution of toluene solution and cooled to 0°C in an ice bath and added to the diazonium solution drop wise over 30 minutes. The reaction mixture was stirred for 24 hours at room temperature. The mixture was quenched with a saturated solution of sodium bicarbonate and resulting solution was extracted with ethyl acetate. The organic layers was collected, dried over sodium sulphate and then filtered. The cure was purified by column chromatography on a silica gel column with a mobile phase of hexane: ethyl acetate (9.5:0.5 v/v).

**c:** Yield: 0.130 g,  $^1\text{H}$  NMR (400 MHz,  $\text{CDCl}_3$ ):  $\delta$  = 7.59 (s, 1H, aromatic), 7.29–7.13 (m, 3H, aromatic), 4.51 (s, 2H, Ferrocene), 4.22 (s, 2H, Ferrocene), 3.91 (s, 5H, Ferrocene).  $^{13}\text{C}$  (100 MHz,  $\text{CDCl}_3$ ):  $\delta$  140.7, 137.0, 129.0, 125.0, 124.9, 84.9, 69.6, 69.1, and 66.7.

**d:** Yield: 0.178 g,  $^1\text{H}$  NMR (400 MHz,  $\text{CDCl}_3$ ):  $\delta$  = 7.42 (s, 4H, aromatic), 4.61 (s, 2H, Ferrocene), 4.31 (s, 2H, Ferrocene), 4.03 (s, 5H, Ferrocene).  $^{13}\text{C}$  (100 MHz,  $\text{CDCl}_3$ ):  $\delta$  139.1, 134.2, 128.6, 126.6, 84.3, 69.6, 69.2 and 66.5.

**General procedure for the synthesis of 3a–d:** 6-bromo-2-butyl-benzo[de]isoquinoline-1,3-dione 2 (100 mg, 0.301mmol), ferrocenyl phenol or ferrocenyl thiophenol (0.316 mmol) and potassium carbonate (124 mg, 0.903mmol) and dry N,N-dimethylformamide (10 mL) were stirred at 120°C for overnight. Upon completion of the reaction, the mixture was cooled and N,N-dimethylformamide was evaporated under vacuum and the obtained crude solid was extracted with dichloromethane (50 x 2) and dried on sodium sulphate and dichloromethane was evaporated under vacuum to obtain the residue. Then the residue was purified on silica gel column chromatography employing hexane: ethyl acetate (19:1, V/V).

**3a:** Yield: 0.118 g, 74 %,  $^1\text{H}$  NMR (400 MHz,  $\text{CDCl}_3$ ):  $\delta$  = 8.74 (d,  $J=8.28$ , 1H, aromatic), 8.67 (d,  $J=7.02$ , 1H, aromatic), 8.47 (d,  $J=8.28$ , 1H, aromatic), 7.80 (t,  $J=7.52$ , 1H, aromatic), 7.42–7.30 (m, 2H, aromatic), 7.28 (s, 1H, aromatic), 7.00–6.95 (m, 2H, aromatic), 4.63 (s, 2H, Ferrocene), 4.34 (s, 2H, Ferrocene), 4.18 (t, 2H,  $J=7.52$ ,  $-\text{NCH}_2$ ), 4.05 (s, 5H, Ferrocene), 1.75–1.68 (m, 2H,  $-\text{CH}_2$ ), 1.50–1.40 (m, 2H,  $-\text{CH}_2$ ), 0.97 (t,  $J=7.27$ , 3H,  $-\text{CH}_3$ ).  $^{13}\text{C}$  (100 MHz,  $\text{CDCl}_3$ ):  $\delta$  164.5, 163.7, 159.9, 154.8, 142.5, 132.7, 131.8, 130.2, 129.6, 128.5, 126.5, 123.8, 123.2, 122.6, 118.2, 117.9, 116.5, 110.4, 83.8, 77.3, 76.9, 76.7, 69.7, 69.4, 66.6, 40.2, 30.2, 20.4, 13.8. HRMS (ESI-TOF):  $m/z$  calculated for  $\text{C}_{32}\text{H}_{27}\text{FeNO}_3$  529.1335  $[\text{M}]^+$ , measured 529.1336  $[\text{M}]^+$ .

**3b:** Yield: 0.123 g, 77 %,  $^1\text{H}$  NMR (400 MHz,  $\text{CDCl}_3$ ):  $\delta$  = 8.71 (d,  $J$  = 8.28, 1H, aromatic), 8.67 (d,  $J$  = 7.02, 1H, aromatic), 8.47 (d,  $J$  = 8.28, 1H, aromatic), 7.79 (t,  $J$  = 7.78, 1H, aromatic), 7.57 (d, 2H,  $J$  = 8.53, aromatic), 7.11 (2H, d,  $J$  = 8.53, aromatic), 6.96 (d, 1H,  $J$  = 8.28 aromatic), 4.65 (s, 2H, Ferrocene), 4.35 (s, 2H, Ferrocene), 4.18 (t, 2H,  $J$  = 7.52,  $-\text{NCH}_2$ ), 4.09 (s, 5H, Ferrocene), 1.76–1.68 (m, 2H,  $-\text{CH}_2$ ), 1.48–1.42 (m, 2H,  $-\text{CH}_2$ ), 0.97 (t,  $J$  = 7.52, 3H,  $-\text{CH}_3$ ).  $^{13}\text{C}$  (100 MHz,  $\text{CDCl}_3$ ): 164.4, 163.7, 159.9, 152.7, 136.9, 132.8, 131.8, 129.6, 128.5, 127.8, 126.4, 123.8, 122.6, 120.7, 116.5, 110.4, 84.4, 69.6, 69.1, 66.5, 40.2, 30.2, 20.4, 13.8. HRMS (ESI–TOF):  $m/z$  calculated for  $\text{C}_{32}\text{H}_{27}\text{FeNO}_3$  529.1335  $[\text{M}]^+$ , measured 529.1337  $[\text{M}]^+$ .

**3c:** Yield: 0.110 g, 67 %,  $^1\text{H}$  NMR (400 MHz,  $\text{CDCl}_3$ ):  $\delta$  = 8.69–8.65 (m, 2H, aromatic), 8.39 (d,  $J$  = 7.78, 1H, aromatic), 7.80 (t,  $J$  = 7.78, 1H, aromatic), 7.64 (s, 1H, aromatic), 7.55 (d, 1H, aromatic), 7.38–7.33 (m, 3H, aromatic), 4.61 (s, 2H, Ferrocene), 4.33 (s, 2H, Ferrocene), 4.16 (t, 2H,  $J$  = 7.02,  $-\text{NCH}_2$ ), 4.00 (s, 5H, Ferrocene), 1.74–1.67 (m, 2H,  $-\text{CH}_2$ ), 1.46–1.42 (m, 2H,  $-\text{CH}_2$ ), 0.97 (t,  $J$  = 7.27, 3H,  $-\text{CH}_3$ ).  $^{13}\text{C}$  (100 MHz,  $\text{CDCl}_3$ ):  $\delta$  163.9, 163.8, 145.1, 141.9, 131.6, 129.9, 129.4, 128.5, 126.9, 126.8, 125.9, 123.2, 120.2, 83.6, 69.6, 69.4, 66.6, 40.2, 30.2, 20.3, 13.8. HRMS (ESI–TOF):  $m/z$  calculated for  $\text{C}_{32}\text{H}_{27}\text{FeNO}_2\text{S}$  545.1107  $[\text{M}]^+$ , measured 545.1103  $[\text{M}]^+$ .

**3d:** Yield: 0.116 g, 70 %,  $^1\text{H}$  NMR (400 MHz,  $\text{CDCl}_3$ ):  $\delta$  = 8.66–8.63 (m, 2H, aromatic), 8.35 (d,  $J$  = 7.78, 1H, aromatic), 7.78 (t,  $J$  = 7.78, 1H, aromatic), 7.55 (d,  $J$  = 8.03, 2H, aromatic), 7.45 (d,  $J$  = 8.28, 2H, aromatic), 7.26 (d,  $J$  = 7.78, 1H, aromatic), 4.68 (s, 2H, Ferrocene), 4.38 (s, 2H, Ferrocene), 4.16 (t, 2H,  $J$  = 7.52,  $-\text{NCH}_2$ ), 4.07 (s, 5H, Ferrocene), 1.74–1.66 (m, 2H,  $-\text{CH}_2$ ), 1.48–1.39 (m, 2H,  $-\text{CH}_2$ ), 0.96 (t,  $J$  = 7.27, 3H,  $-\text{CH}_3$ ).  $^{13}\text{C}$  (100 MHz,  $\text{CDCl}_3$ ):  $\delta$  164.0, 163.9, 145.7, 141.5, 134.6, 131.6, 130.8, 130.1, 129.1, 128.4, 127.5, 126.9, 126.8, 125.2, 123.2, 119.8, 83.5, 69.7, 69.5, 66.7, 40.2, 30.2, 20.3, 13.8. HRMS (ESI–TOF):  $m/z$  calculated for  $\text{C}_{32}\text{H}_{27}\text{FeNO}_2\text{S}$  545.1107  $[\text{M}]^+$ , measured 545.1119  $[\text{M}]^+$ .

**General procedure for the synthesis of 3e,f:** 6-bromo-2-butyl-benzo[de]isoquinoline-1,3-dione **2** (100 mg, 0.301 mmol), ferrocenyl aniline (92 mg, 0.3162 mmol), tris-(dibenzylideneacetone)-dipalladium(0) (27 mg, 0.0301 mmol), tris-tert-butylphosphine (30 mg, 0.150 mmol), sodium-tert-butoxide (58 mg, 0.60 mmol) and dry toluene (15 mL) were refluxed at under argon overnight. After cooling, the reaction mixture was evaporated in vacuo and purified by a column chromatography on silica gel using dichloromethane as an eluent.

**3e:** Yield: 0.101 g, 63 %,  $^1\text{H}$  NMR (400 MHz,  $\text{CDCl}_3$ ):  $\delta$  = 8.64 (d,  $J$  = 7.27, 1H, aromatic), 8.44 (d,  $J$  = 8.53, 1H, aromatic), 8.34 (d,  $J$  = 8.28, 1H, aromatic), 8.01 (s, 1H, Ar), 7.72 (t,  $J$

=7.53, 1H, aromatic), 7.40–7.33 (m, 2H, aromatic), 7.14–7.12 (d,  $J=6.77$ , 1H, aromatic), 6.86 (s, 1H, –NH), 4.63 (s, 2H, Ferrocene), 4.34 (s, 2H, Ferrocene), 4.17 (t, 2H,  $J=7.27$ , –NCH<sub>2</sub>), 4.07 (s, 5H, Ferrocene), 1.75–1.68 (m, 2H, –CH<sub>2</sub>), 1.47–1.40 (m, 2H, –CH<sub>2</sub>), 0.97 (t,  $J=7.27$ , 3H, –CH<sub>3</sub>). <sup>13</sup>C (100 MHz, CDCl<sub>3</sub>):  $\delta$  164.5, 163.9, 162.5, 146.7, 141.5, 139.9, 133.4, 131.4, 129.9, 129.7, 126.4, 125.5, 123.3, 122.7, 121.9, 119.8, 113.4, 109.1, 84.3, 69.6, 69.2, 62.5, 40.1, 30.2, 20.4, 13.8. HRMS (ESI–TOF):  $m/z$  calculated for C<sub>32</sub>H<sub>28</sub>FeN<sub>2</sub>O<sub>2</sub> 528.1495 [M]<sup>+</sup>, measured 528.1493 [M]<sup>+</sup>.

**3f**: Yield: 0.108 g, 68 %, <sup>1</sup>H NMR (400 MHz, CDCl<sub>3</sub>):  $\delta$  = 8.63 (d,  $J=7.27$ , 1H, aromatic), 8.44 (d,  $J=8.28$ , 1H, aromatic), 8.30 (d,  $J=8.28$ , 1H, aromatic), 7.71 (t,  $J=7.78$ , 1H, aromatic), 7.53 (d,  $J=8.28$ , 2H, aromatic), 7.34 (d,  $J=8.53$ , 1H, aromatic), 7.24 (d,  $J=8.28$ , 1H, aromatic), 6.81 (s, 1H, –NH), 4.65 (s, 2H, Ferrocene), 4.34 (s, 2H, Ferrocene), 4.17 (t, 2H,  $J=7.52$ , –NCH<sub>2</sub>), 4.08 (s, 5H, Ferrocene), 1.75–1.68 (m, 2H, –CH<sub>2</sub>), 1.49–1.42 (m, 2H, –CH<sub>2</sub>), 0.97 (t,  $J=7.52$ , 3H, –CH<sub>3</sub>). <sup>13</sup>C (100 MHz, CDCl<sub>3</sub>):  $\delta$  164.5, 163.9, 146.6, 137.4, 136.2, 133.5, 131.4, 127.3, 126.2, 125.4, 123.3, 122.5, 113.2, 108.8, 84.7, 69.6, 69.0, 63.3, 40.1, 30.3, 20.4, 13.9. HRMS (ESI–TOF):  $m/z$  calculated for C<sub>32</sub>H<sub>28</sub>FeN<sub>2</sub>O<sub>2</sub> 528.1495 [M]<sup>+</sup>, measured 528.1506 [M]<sup>+</sup>.

### References:

- (1) (a) S. Elinger, K. R. Graham, P. Shi, R. T. Farley, T. T. Steckler, N. R. Brookins, P. Taranekar, J. Mei, A. L. Padilha, R. T. Ensley, H. Hu, S. Webster, J. D. Hagan, V. E. W. Stryland, S. K. Schanze and R. J. Reynolds, *Chem. Mater.*, 2011, **23**, 3805–3817; (b) J. Yang, D. Yan and S. T. Jones, *Chem. Rev.*, 2015, **115**, 5570–5603; (c) M. O. Neill and S. M. Kelly, *Adv. Mater.*, 2011, **23**, 566–584; (d) K. Asadi, M. Y. Li, P. W. M. Blom, M. Kemerink and D. M. de Leeuw, *Mater. Today.*, 2011, **14**, 592–599; (e) A. N. Sokolov, B. C. K. Tee, C. J. Bettinger, J. B. H. Tok and Z. N. Bao, *Acc. Chem. Res.*, 2012, **45**, 361–371; (f) C. L. Wang, H. L. Dong, W. P. Hu, Y. Q. Liu and D. B. Zhu, *Chem. Rev.*, 2011, **112**, 2208–2267; (g) A. Vecchi, P. Galloni, B. Floris, S. V. Dudkin and N. V. Nemykin, *Coord. Chem. Rev.*, 2015, **291**, 95–171; (h) H. Liu, J. Xu, Y. Li and Y. Li, *Acc. Chem. Res.*, 2010, **43**, 1496–1508; (i) N. Kraube, M. Kielmann, J. Ma and H. Butenschon, *Eur. J. Org. Chem.*, 2015, **2015**, 2622–2631; (j) J. Ma, N. Kraube and H. Butenschon, *Eur. J. Org. Chem.*, DOI: 10.1002/ejoc.201500483; (k) N. Kraube and H. Butenschon, *H. Synlett.*, 2015, **26**, 1450–1454.
- (2) (a) M. D. Rebecca, B. V. Emma, M. P. Frederick, E. K. Paul and G. Thorfinnur, *Chem. Soc. Rev.*, 2010, **39**, 3936–3953; (b) B. Swagata, B. V. Emma, M. P. Caroline, A. M. Samantha, M. T. Gillian, J. G. Lisa, O. F. Daniel, M. K. John and G. Thorfinnur, *Chem. Soc. Rev.*, 2013, **42**, 1601–1618.

- (3) (a) A. Pardo, L. M. J. Poyato and E. Martin, *J. Photo. Chem.*, 1987, **36**, 323–329; (b) A. Pardo, E. Martin, L. M. J. Poyato, J. J. Camacho, M. F. Brana and M. J. Castellano, *J. Photochem. Photobiol. A.*, 1987, **41**, 69–78.
- (4) D. Kolosov, V. Adamovich, P. Djurovich, E. M. Thompson and C. Adachi, *J. Am. Chem. Soc.*, 2002, **124**, 9945–9954.
- (5) I. Grabchev, I. Moneva, V. Bojinov and S. Guittonneau, *J. Mater. Chem.* 2000, **10**, 1291–1296.
- (6) (a) R. N. Chereddy, V. M. Niladi Raju, P. Nagaraju, R. V. Krishnaswamy, S. P. Korrapati, R. P. Bangal and V. J. Rao, *Analyst.*, 2014, **139**, 6352; (b) Y. Kai, Y. Hu, W. Kai, W. Zhi, M. Liang and W. Yang, *Spectro Chimica Acta part A: Molecular and Biomolecular Spectroscopy.*, 2014, **118**, 239–243.
- (7) J. Zhang, G. Li, C. Kang, H. Lu, X. Zhao, C. Li, W. Li and Z. Bo, *Dyes and Pigments.*, 2015, **115**, 181–189.
- (8) (a) M. Verma, V. Luxami and K. Paul, *RSC Adv.*, 2015, **5**, 41803–41813; (b) S. Murphy, A. S. Bright, E. F. Poynton, Mc. T. Cabe, A. J. Kitchen, B. V. Emma, C. D. Williams and T. Gunnlaugsson, *Org. Biomol. Chem.*, 2014, **12**, 6610–6623.
- (9) (a) M. Lee, S. Jo, D. Lee, Z. Xu and J. Yoon, *Dyes and Pigments.*, 2015, **120**, 288–292; (b) H. Lee, M. H. Jeon, H. J. Han, N. Park, C. Kang and L. J. Sessler, *J. Am. Chem. Soc.*, 2014, **136**, 8430–8437.
- (10) (a) S. Saha and A. Samanta, *J. Phys. Chem. A.*, 2002, **106**, 4763–4771; (b) T. Philipova, I. Karamancheva and I. Grabche, *Dyes and Pigments.*, 1995, **28**, 91–99.
- (11) (a) H. Ulla, R. M. Kiran, B. Garudachari, N. M. Satyanarayan, G. Umesh and M. A. Isloor, *Optical Materials.*, 2014, **37**, 311–32;. (b) J-A. Gan, L. Q. Song, Y. X. Hou, C. K. Chen and H. Tian, *J Photochem. Photobiol. A.*, 2004, **162**, 399–406; (c) Y. Wang, X. Zhang, B. Han, J. Peng, S. Hou, Y. Huang, H. Sun, M. Xie and Z. Lu, *Dyes and Pigments.*, 2010, **86**, 190–196.
- (12) (a) T. Jadhav, R. Maragani, R. Misra, V. Sreeramulu, D. N. Rao and S. M. Mobin, *Dalton Trans.*, 2013, **42**, 4340–4342; (b) R. Misra, R. Maragani, K. R. Patel and G. D. Sharma, *RSC. Adv.*, 2014, **4**, 34904–34911; (c) R. Maragani and R. Misra, *Tetrahedron.*, 2014, **70**, 3390–3399; (d) C. P. Singh, R. Sharma, V. Shukla, P. Khundrakpan, R. Misra, K. S. Bindra and R. Chari, *Chem. Phys. Lett.*, 2014, **616–617**, 189–195; (e) P. Gautam, B. Dhokale, V. Shukla, C. P. Singh, K. S. Bindra and R. Misra, *J Photochem. Photobiol. A.*, 2012, **239**, 24–27; (f) E. Maligaspe, T. J. Pundsack, L. M. Albert, Y. V. Zatsikha, P. V. Solntsev, D. A. Blank and V. N. Nemykin, *Inorg. Chem.*, 2015, **54**, 4167–4174; (g) B. Sun, Z.

- Ou, D. Meng, Y. Fang, Y. Song, W. Zhu, P. V. Solntsev, V. N. Nemykin and K. M. Kadish, *Inorg. Chem.*, 2014, **53**, 8600-8609; (h) C. J. Ziegler, K. Chanawanno, A. Hasheminsasab, Y. V. Zatsikha, E. Maligaspe and V. N. Nemykin, *Inorg. Chem.*, 2014, **53**, 4751-4755.
- (13) C. J. McAdam, B. H. Robinson and J. Simpson, *Organometallics.*, 2000, **19**, 3644–3653.
- (14) C. J. McAdam, J. L. Morgan, B. H. Robinson, J. Simpson, P. H. Rieger and A. L. Rieger, *Organometallics.*, 2003, **22**, 5126–5136.
- (15) C. J. McAdam, R. B. Robinson, J. Simpson and T. Tagg, *Organometallics.*, 2010, **29**, 2474–2483.
- (16) T. Tagg, H. G. Kjaergaard, J. R. Lane, C. J. McAdam, B. H. Robinson and J. Simpson, *Organometallics.*, 2015, **34**, 2662–2666.
- (17) P. Chinapang, V. Ruangpornvisti, M. Sukwattanasinitt and P. Rashatasakhon, *Dyes and Pigments.*, 2015, **112**, 236–238.
- (18) (a) R. Maragani, T. Jadhav, S. M. Mobin and R. Misra, *Tetrahedron.*, 2012, **68**, 7302–7308; (b) B. Dhokale, P. Gautam and R. Misra, *Tetrahedron Lett.*, 2012, **53**, 2352–2354; (c) B. Dhokale, P. Gautam, S. M. Mobin and R. Misra, *Dalton Trans.*, 2013, **42**, 1512–1518; (d) R. Maragani, T. Jadhav, S. M. Mobin and R. Misra, *RSC Adv.*, 2013, **3**, 2889–2892; (e) R. Misra, B. Dhokale, T. Jadhav and S. M. Mobin, *Dalton Trans.*, 2013, **42**, 13658–13666; (f) R. Sharma, P. Gautam, S. M. Mobin and R. Misra, *Dalton Trans.*, 2013, **42**, 5539–5545; (g) R. Misra, R. Sharma and S. M. Mobin, *Dalton Trans.*, 2014, **43**, 6891–6896; (f) R. Misra, T. Jadhav and S. M. Mobin, *Dalton Trans.*, 2014, **43**, 2013–2022; (g) P. Gautam, B. Dhokale, S. M. Mobin and R. Misra, *RSC Adv.*, 2012, **2**, 12105–12107.
- (19) R. Misra, B. Dhokale, T. Jadhav and S. M. Mobin, *Organometallics.*, 2014, **33**, 1867–1877.
- (20) W. W. Zhang, Y. G. Yu, Z. D. Lu, W. L. Mao, Y. Z. Li and Q. J. Meng, *Organometallics.*, 2007, **26**, 865–873.
- (21) (a) A. D. Becke, *J. Chem. Phys.*, 1993, **98**, 5648–5652; (b) C. T. Lee, W. T. Yang and R. G. Parr, *Phys. Rev. B.*, 1988, **37**, 785–789; (c) P. Hay and W. R. Wadt, *J. Chem. Phys.*, 1985, **82**, 270–283.
- (22) (a) M. M. Francl, W. J. Pietro, W. J. Hehre, J. S. Binkley, M. S. Gordon, D. J. Defrees and J. A. Pople, *J. Chem. Phys.*, 1982, **77**, 3654–3665; (b) F. Ding, S. Chen and H. Wang, *Materials.*, 2010, **3**, 2668–2683.